Stellar krypton cross sections at $kT = 25$ and 52 keV

F. Käppeler

Kernforschungszentrum Karlsruhe, Institut für Kernphysik, D-7500 Karlsruhe, Federal Republic of Germany

A. A. Naqvi and M. Al-Ohali

University of Petroleum and Minerals, Dhahran, Saudi Arabia

(Received 21 October 1986)

Studies of neutron capture nucleosynthesis in the s process usually refer to a thermal energy of $kT = 30$ keV, corresponding to a temperature of $T = 3.5 \times 10^8$ K. This convention is justified as stellar neutron capture rates are in general not sensitive to temperature because of the approximate $E_n^{-1/2}$ dependence of most capture cross sections. But several important exceptions of this rule require more detailed information on the variation of the average stellar cross section with temperature. We show that activation measurements can be performed in a quasistellar neutron spectrum for $kT = 52$ keV, using kinematically collimated neutrons from the ^{3}H(p,n) reaction. Neutron capture cross sections were measured in this spectrum and at $kT = 25$ keV for ^{86}Kr(n,γ) and for the reaction ^{84}Kr(n,γ)^{85}Kr^m, which populates the isomeric state in ^{85}Kr. In this way, the respective 30 keV cross sections of 3.5 ± 0.3 and 16.7 ± 1.2 mb could be derived by *inter*polation.

I. INTRODUCTION

By convention, stellar neutron capture rates for s-process studies are based on a common constant thermal energy of $kT = 30$ keV, corresponding to a temperature of $T = 3.5 \times 10^8$ K. This apparent simplification is justified—in spite of the possible range of temperatures between 200×10^6 and 400×10^6 K as proposed for different stellar s-process models—because the stellar neutron capture rates are nearly temperature-independent. These rates

$$\lambda_n = n_n \langle \sigma \rangle v_T \tag{1}$$

are determined by the neutron density, n_n, and the neutron capture cross sections, $\langle \sigma \rangle$, averaged over the thermal Maxwell-Boltzmann energy distribution. In general, these Maxwellian averaged cross sections exhibit to first order an $E_n^{-1/2}$ dependence on neutron energy, which is just compensated for by the thermal velocity, v_T, in Eq. (1).

The Maxwellian averaged cross sections are normally derived from experimentally measured differential data, $\sigma(E_n)$, by proper folding with the thermal spectrum. Differential cross sections are obtained in time-of-flight (TOF) experiments using so called direct detection techniques for registration of the γ rays released by neutron capture (see, e.g., Gibbons and Macklin,[1] and Käppeler, Wisshak, and Hong[2]). An important complement to the direct detection methods was described by Beer and Käppeler,[3] who showed that a thermal neutron spectrum for $kT = 25$ keV could be imitated almost perfectly using kinematically collimated neutrons from the ^{7}Li(p,n)^{7}Be reaction near threshold. (In Ref. 3, a value of $kT = 23.4$ keV is quoted, which was later revised.[4]) Hence, activation measurements in such a spectrum yield directly the required "stellar" cross sections. This method is restricted to those cases where neutron capture leads to an unsta-

ble isotope which can be identified by its decay properties, but it offers two important merits.

(i) The *high sensitivity* allows for an accurate determination of small cross sections even if only small amounts of sample material are available.

(ii) The use of high resolution gamma-ray detectors for activity counting makes it *selective* for the particular final state; this means that measurements can be performed on natural samples or on samples with only moderate isotopic enrichment, and—even more important—that one can distinguish between the partial cross sections to the ground state and to long-lived isomeric states. In fact, the activation method is the only technique for an experimental determination of isomeric ratios (see below).

The results for $kT = 25$ keV obtained with this activation technique have to be extrapolated to the standard value $kT = 30$ keV. Assuming an $E_n^{-1/2}$ dependence, the associated uncertainty is less than 5% for most isotopes[5] and thus smaller than or comparable to the systematic uncertainties of most differential data. In view of future needs of more precise cross sections for improved s-process analyses, however, it is indispensible to reduce or even eliminate this extrapolation uncertainty. Beside the need for better precision, information on the energy dependence of stellar cross sections is of direct importance in those cases that deviate significantly from the common energy dependence: The cross sections of nuclei near magic neutron numbers are characterized by few resonances in the energy range around 30 keV, which may well result in a nontypical energy dependence of the Maxwellian average. These isotopes act as bottle necks in the neutron capture path of the s process because of their small cross section values which therefore are required with high precision. In Sec. III we describe a measurement on ^{86}Kr, which falls in this category. Other exceptions are the aforementioned isomeric ratios

$$R_{\text{iso}} = \frac{\text{partial capture cross section to isomer}}{\text{total capture cross section}} \ . \quad (2)$$

Their relevance for the s process comes from the fact that some of the branchings in the neutron capture path depend critically on the probability for populating the isomeric state.[6] In Sec. III we discuss this problem in detail for ^{85}Kr. Before that, we show in Sec. II that the ^{3}H(p,n)^{3}He reaction can be used to produce a neutron spectrum very near the thermal distribution for $kT = 52$ keV. Measurements at both energies, $kT = 25$ and 52 keV, then allow for interpolation to $kT = 30$ keV with considerably improved reliability.

II. SIMULATION OF A MAXWELLIAN NEUTRON SPECTRUM AT $kT = 52$ keV

The successful approximation of a thermal neutron spectrum for $kT = 25$ keV by means of the ^{7}Li(p,n) reaction (Beer and Käppeler[3]) initiated the present study of the ^{3}H(p,n) reaction. In analogy to the lithium case, the proton energy was restricted to values near the reaction threshold leading to kinematically collimated neutrons in the forward direction. The measurements were carried out at the Karlsruhe 3.75 MV Van de Graaff accelerator using a pulsed proton beam for neutron energy determination via TOF. The experimental setup is sketched in Fig. 1, consisting of a tritium loaded titanium layer for neutron production, a movable ^{6}Li-glass detector for measuring the neutron spectrum at different angles, and a stationary ^{6}Li-glass detector which served as a monitor for normalization of the various spectra to the same overall neutron yield. The forward collimation of the neutrons through the reaction kinematics is an important advantage for the later use in activation measurements because corrections due to scattered neutrons are minimized.

This advantage is lost at higher proton energies, where the neutron cone widens rapidly till the backward threshold is reached. In the course of our investigations we found that thermal spectra can be produced via the ^{7}Li(p,n) reaction also at these higher proton energies. For example, with $E_p = 1970$ keV, one obtains a spectrum similar to a Maxwell-Boltzmann distribution for $kT = 34$ keV, provided that the measurement is restricted to a for-

ward cone of 120 deg opening angle. Though the intensities emitted at larger angles are comparatively small, their effect would be difficult to quantify. Therefore, we will not pursue this possibility further. For the sake of clean experimental conditions we favor, instead, measurements with kinematic collimation which have the advantage that the spectrum is precisely defined in neutron energy as well as in geometry.

The tritium target that was available for our present investigation was originally designed for TOF measurements and was not optimal for activations. While the target used by Beer and Käppeler[3] consisted simply of an evaporated metallic lithium layer on a laterally cooled copper disk of 0.5 mm thickness, the construction which is sketched schematically in Fig. 1 was adapted to commercially available tritium targets. These are tritium loaded titanium layers (1.0 mg cm^{-2}) evaporated on a 0.3 mm thick tungsten disk. For improvement of the lifetime and for reduction of tritium losses, the target was covered by an additional aluminum layer of 50 μg cm^{-2} thickness. The specific target activity was 3×10^{10} bq cm^{-2}. The cooling water flows in a 0.8 mm wide gap between the W backing and the 0.1 mm thick outer window of stainless steel.

The transmission of this target for 30 keV neutrons is 89%, significantly lower than the 96% of the above mentioned lithium targets. By far, most of the neutrons that interact with the target are scattered at the hydrogen nuclei of the cooling water thereby losing a considerable fraction of their energy. As a result, the average spectrum of the scattered neutrons is slightly softer. This effect has no strong impact on the TOF determination of the neutron spectrum as described below, but needs to be considered in cross section measurements where it may cause a systematic uncertainty. This can be avoided if the simpler construction of the ^{7}Li targets would also be used for tritium.

Another problem with the present tritium target concerns the lower integral neutron yield which results from the smaller (p,n) cross section of the ^{3}H(p,n) reaction, the dilution of tritium in the titanium matrix, and from the fact that this target can only be exposed to proton currents of ~ 50 μA. These limitations are partly compensated for by the broader neutron energy spectrum, leading to typically integral neutron source strengths of 10^8 s^{-1} compared to $(1-2) \times 10^9$ s^{-1} for the lithium targets.

During the spectrum measurements the accelerator was operated in pulsed mode at a repetition rate of 1 MHz, a pulse width of 18 ns, and with beam currents of 2 μA. Neutron TOF spectra were recorded for both detectors simultaneously with the movable detector being placed at 0, 15, 30, 45, and 60 deg in subsequent runs. The monitor spectrum served to ensure constant proton beam conditions throughout the entire experiment.

The original TOF spectra measured with the movable detector were corrected for backgrounds, normalized to the integral yield of the respective monitor spectrum, and transformed to a neutron energy scale. Then, correction for the energy-dependent efficiency of the ^{6}Li-glass detector yielded the spectra of Fig. 2. That neutrons are still
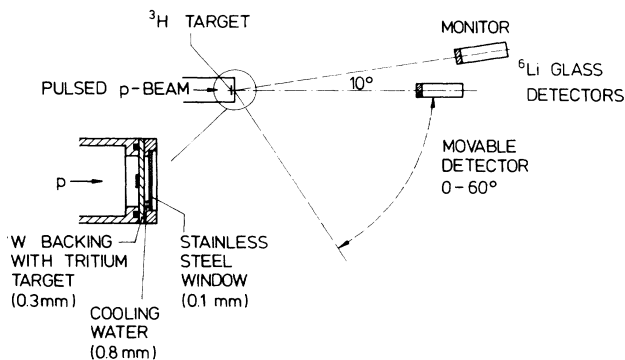

FIG. 1. Schematic sketch of the experimental setup. The inset shows the tritium target in detail.
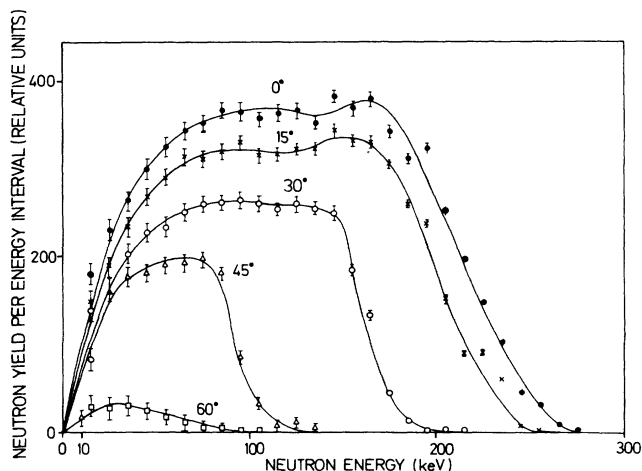
FIG. 2. Neutron spectra from the ^{3}H(p,n)^{3}He reaction at $E_p = 1099$ keV. The spectra are taken at different angles with respect to the proton beam.
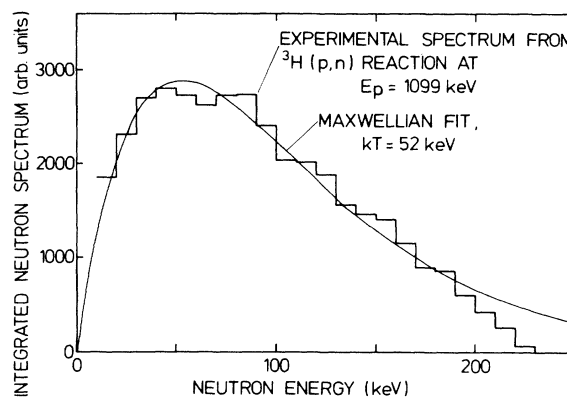

FIG. 3. Angle-integrated neutron spectrum from the ^{3}H(p,n)^{3}He reaction at $E_p = 1099$ keV (histogram). The best Maxwell-Boltzmann fit to the experimental distribution was obtained for $kT = 52$ keV.

observed at 60 deg (though the maximum angle is nominally 54 deg at this energy) is mostly because of small angle scattering of protons in the target.

The last step of data processing comprised unfolding of the experimental resolution function and integration over the entire neutron cone. The best representation of a Maxwell-Boltzmann distribution was found for a proton energy $E_p = 1099$ keV, 80 keV above the threshold of the ^{3}H(p,n) reaction. This value already includes an 8 keV correction for the energy loss in the aluminum protection layer of the tritium target. Figure 3 shows the resulting integral spectrum (histogram) together with the fit for $kT = 52$ keV. The true overlap between the two distributions amounts to 91% with most of the remaining difference being due to the fact that the experimental spectrum ends at $E_n^{max} = 225$ keV. However, in cross section measurements, this upper end of the spectrum contributes very little as the cross sections decrease at higher energies.

III. CROSS SECTION MEASUREMENTS

A. Experiment and data analysis

Both cross sections, the total capture cross section of ^{86}Kr as well as the partial cross section of ^{84}Kr to the

isomeric state of ^{85}Kr, were measured via activation for $kT = 25$ keV and for $kT = 52$ keV. The experimental set-up was the same as described by Beer and Käppeler,[3] with the samples directly attached to the respective neutron target. The neutron yield was monitored throughout the activations for later determination of the fraction of activated nuclei that decayed already during the irradiations. Before each activation, the correct proton energy was verified experimentally by a TOF measurement of the respective maximum neutron energy of 106 and 225 keV. Then, the accelerator was switched to direct current (dc) mode without changing the proton energy. After the irradiations, the samples were removed from the accelerator for activity counting in a low background environment.

The samples consisted of natural and enriched krypton trapped in the crystal lattice of zeolite 5A with concentrations of typically 50 cm^3 krypton per gram zeolite; for a technical discussion see Penzhorn, Walter, and Beer.[7] To obtain quantitative estimates for the associated systematic uncertainties, the relevant sample parameters were chosen to vary over a significant range. This included the zeolite type, krypton loading, isotopic composition, and the sample thickness. The krypton samples were sandwiched between gold foils of the same diameter of 6 mm. The

TABLE I. Sample characteristics. NTP denotes normal temperature and pressure.

| Sample	Composition Chemical	Isotopic	Investigated isotope	Effective thickness for the investigated isotope (mm)	(nuclei/b) × 10^4	Mass of the investigated isotope (mg)
Kr-I	Mg-zeolite (52.8±1.33 cm^3 NTP/g)	natural	^{84}Kr ^{86}Kr	1.0	1.68 0.51	6.59±2.5% 2.00±2.5%
Kr-II	Ca-zeolite (48.0±0.8 cm^3 NTP/g)	natural	^{84}Kr ^{86}Kr	0.5	0.86 0.26	3.37±1.7% 1.02±1.7%
Kr-III	Ca-zeolite (18.6±0.4 cm^3 NTP/g)	^{86}Kr 99.5% ^{84}Kr 0.5%	^{86}Kr	1.3	1.36	5.47±2.0%
Au-1—16	metal foils	natural	^{197}Au	0.012—0.030	0.69—1.7	6.4—16.2
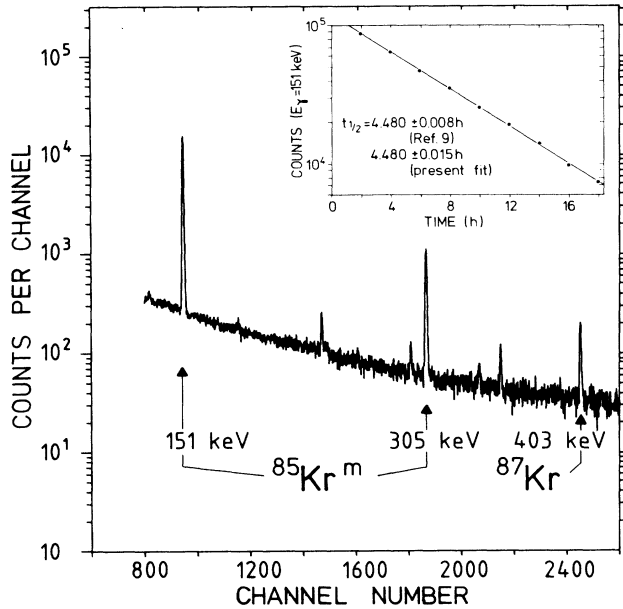
FIG. 4. Gamma-ray spectrum measured after activation of a natural krypton sample. The transitions at 151 and 305 keV originate from the decay of the isomer ^{85}Kr^m, while the 403 keV line stems from the decay of ^{87}Kr. The inset shows the intensity of the 151 keV line as a function of time.

simultaneous activation of the gold foils served for normalization to the well known gold cross section. The characteristics of all samples used in the activations are listed in Table I.

Different irradiation times were chosen for the various activations in order to verify the proper correction for the fraction of nuclei that decayed during the activation. In this respect it was important that the effect of the different half-lives of the krypton isotopes and of ^{198}Au was considered via the recorded time-dependence of the neutron yield (see Ref. 3).

After the activations, the induced activities were measured for each sample separately using a shielded Ge detector with 1.6 keV resolution at $E_\gamma=514$ keV. Figure 4 presents the gamma-ray spectrum measured after activation of a natural krypton sample at $kT=25$ keV. The sensitivity of the activation method yields the cross sec-

TABLE II. Decay properties of the relevant product nuclei [all data from Lederer and Shirley (see Ref. 9)].

Product nucleus	Half-life $t_{1/2}$	Gamma-ray energy E_γ (keV)	Gamma rays per decay I_γ (%)
^{85}Kr^m	4.48 h	151	75.3±3.3
		305	14.0±0.4
^{87}Kr	76.3 min	403	50.0±3.0
^{198}Au	2.696 d	412	95.5±0.5

TABLE III. Gold reference cross sections.

Thermal energy kT (keV)	^{197}Au reference cross section (mb)
30	562±20[a]
25	619±22[b]
52	431±15[b]

[a]Recommended value of Bao and Käppeler (1986).
[b]Calculated from the differential cross sections of Macklin (1982), normalized to the $kT=30$ keV value.

tions of both reactions simultaneously. The spectrum clearly exhibits gamma-ray transitions from the decay of the reaction products ^{87}Kr and ^{85}Kr^m. The two gamma-ray lines at 151 and 305 keV from the latter decay differ sufficiently in energy and intensity to require significantly different corrections, e.g., for background, gamma-ray self absorption, and Ge-detector efficiency. The proper treatment of these corrections is verified by the consistent cross sections obtained in this way (Table V). The inset of Fig. 4 shows the intensity of the 151 keV line as a function of time. The reproduction of the 4.48 h half-life of the ^{85}Kr isomer by a fit to the measured points (solid line) confirms the background subtraction and excludes any overlapping background line. The lower neutron yield at $kT=52$ keV does not allow for the same sensitivity as is shown in Fig. 4. In particular, an enriched ^{86}Kr sample is required in order to achieve reasonable statistics for the 403 keV line from the ^{87}Kr decay.

In addition to the measured quantities, further input data were adopted from literature. The corrections for gamma-ray self-absorption in the samples were calculated using the tables of Veigele,[8] and the relative gamma-ray yields for the decay of ^{85}Kr^m, ^{86}Kr, and ^{198}Au were taken from Lederer and Shirley[9] (Table II). The ^{197}Au reference cross sections for $kT=25$ and 52 keV were calculated from the revised[10] differential gold cross section of Mack-

TABLE IV. Systematic experimental uncertainties.

Source of uncertainty	Relative contribution to Maxwellian average (%)
Au standard cross section	3.5
Activation via scattered neutrons	<3
Neutron flux dispersion including neutron multiple scattering and self-absorption	2.8—7.1
Irradiation history	<2
Deviation of neutron spectrum from Maxwellian shape	<2
Absolute gamma-ray intensity per decay	3—6
Ge(Li) efficiency	2
Gamma ray self-absorption in sample	<1
Total systematic uncertainties	6.5—11.7

lin, Halperin, and Winters,[11] and normalized to the recommended Maxwellian average for $kT = 30$ keV (Ref. 5) for which an uncertainty of 3.5% is assumed (Table III).

The systematic uncertainties of activation measurements in a simulated stellar spectrum have been discussed elsewhere.[3,12] Several components have since been improved, e.g., the efficiency of the Ge detector, while a slightly higher uncertainty of the gold cross section should be considered at present. The effect of scattered neutrons is only significant for the distribution with $kT = 52$ keV and was estimated to contribute a systematic uncertainty of ~3%. The large uncertainties caused by the observed neutron flux dispersion are because of the rather thick zeolite samples. The uncertainty, because of counting statistics is almost negligible compared to the systematic errors. Table IV summarizes the various systematic uncertainties of the present measurements.

B. Results, cross sections at $kT = 30$ keV, and astrophysical implications

The results obtained in the different activations are compiled in Table V together with the corresponding statistical and systematic uncertainties. Four activations were performed at $kT = 25$ and 52 keV, respectively. Sample Kr-I was used in activations 1—5, sample Kr-II in activation 6, and the enriched sample Kr-III in activations 7 and 8. At $kT = 25$ keV, the partial cross section ^{84}Kr(n,γ)^{85}Kr^m could be consistency derived from the two transitions at 151 and 305 keV, but the statistics of the weaker 305 keV line were not always sufficient at $kT = 52$ keV. The lower neutron yield from the ^{3}H(p,n)^{3}He reaction did not allow to deduce the small ^{86}Kr cross section from the activations with natural samples as at 25 keV, but definitely required an enriched sample. The systematic uncertainties—which clearly dominate over counting statistics—determined the accuracy of the present results to ~7%. Within these limits, there is good agreement be-

tween the results obtained in different activations under different conditions.

The energy dependence of the partial cross section of ^{84}Kr was found to scale with $E_n^{-0.8}$, leading to an interpolated value of 16.7 ± 1.2 mb at the standard thermal energy of $kT = 30$ keV. The additional uncertainty from the interpolation is 3%, whereas a $1/v$ extrapolation of the measured value from $kT = 25$ keV would result in a 6% error. The ^{86}Kr cross section does not show any significant dependence on neutron energy in the investigated range, indicating a pronounced resonance structure due to the magic neutron number $N = 82$. Consequently, a 30 keV cross section of 3.5 ± 0.3 mb is appropriate, in agreement with a previous activation,[13] which gave 3.8 ± 0.7 mb. Differential cross section measurements reported consistently higher values of 4.8 ± 1.2 mb (Ref. 14) and of 5.6 ± 0.7 mb (Ref. 15), a discrepancy which might reflect the background problems near the sensitivity limit of these techniques.

The isomeric ratio of ^{85}Kr as defined in Eq. (2) can be determined from the present results if the total capture cross section of ^{84}Kr is adopted from literature. The only existing differential measurement by Walter et al.[15] was renormalized for a revision of the gold reference cross section[10] and averaged for $kT = 25$ and 52 keV, yielding 39.6 ± 4.5 and 25.9 ± 2.9 mb, respectively. With these values one obtains for the isomeric ratios

$$R_{iso} = 0.49 + 0.06 \quad (kT = 25 \text{ keV}) ,$$

and

$$R_{iso} = 0.42 + 0.06 \quad (kT = 52 \text{ keV}) .$$

Hence, the isomeric ratio is practically constant in the range of s-process temperatures with an interpolated value of 0.48 ± 0.06 at $kT = 30$ keV. The comparison of the present 30 keV values with previous data (Table VI) shows that the experimental uncertainties could be reduced considerably. Note that the large discrepancy for the partial cross section of ^{84}Kr results mostly from the $1/v$ extrapo-

TABLE V. Results obtained in activations with modified parameters and final cross sections.

Neutron spectrum	Reaction	Activation number	Gamma-ray line (keV)	σ (mb)	$\Delta\sigma_{sys}$ (%)	$\Delta\sigma_{stat}$ (%)	Final cross section (mb)
$kT = 25$ keV	^{84}Kr(n,γ)^{85}Kr^m	1	151	19.1	7.2	0.4	
			305	19.0	6.4	1.0	
		2	151	19.6	7.5	0.4	
			305	20.1	6.6	0.9	
		6	151	19.0	7.4	0.6	
			305	19.3	6.5	1.6	19.3±1.3
	^{86}Kr(n,γ)^{87}Kr	2	403	3.5	8.5	4.0	
		6	403	3.1	8.2	5.0	
		7	403	3.7	8.6	2.3	3.58±0.30
$kT = 52$ keV	^{84}Kr(n,γ)^{85}Kr^m	3	151	10.8	9.3	2.2	
		4	151	10.8	8.3	1.5	
			305	10.5	7.6	6.1	
		5	151	10.7	8.6	3.6	10.7±0.9
	^{86}Kr(n,γ)^{87}Kr	8	403	3.3	11.7	8.7	3.3±0.5

TABLE VI. Maxwellian averaged cross sections for $kT=30$ keV.

	Previous data	This work
^{84}Kr(n,γ)^{85}Kr^m	19.0 ± 2.4[a]	16.7 ± 1.2 (mb)
^{86}Kr(n,γ)^{87}Kr	3.8 ± 0.7[b]	3.5 ± 0.3 (mb)
R_{iso}(^{84}Kr)	0.57 ± 0.10[c]	0.49 ± 0.06

[a]Reference 5, based on $1/v$ extrapolation from $kT=25$ keV.
[b]Reference 13.
[c]Calculated from data of Ref. 5.

lation used in Ref. 5. If the proper energy dependence from this work is used instead, one obtains a 30 keV value of 18.0 ± 2.4 mb, in much better agreement with the new cross section of 16.7 ± 1.2 mb.

Recently, the s-process branching at ^{85}Kr was investigated by Walter et al.,[13] who used a ^{86}Kr cross section of 3.8 ± 0.7 mb and an isomeric ratio of 0.57 ± 0.10. As both values agree within errors with the present results, there are no severe implications for the astrophysical results obtained in that work. The lower isomeric ratio reported here leads to a somewhat lower average neutron density for the weak s-process component, but still within the limits given in Ref. 13, $n_n=(0.5-1.3)\times10^8$ cm^{-3}. These limits are mostly determined by the uncertainty of the capture cross section of the branching point isotope ^{85}Kr, for which no experimental value exists so far, and by the correction for the contribution of the main s-process component to this branching.

IV. SUMMARY

The present results can be summarized in three points.
(i) Complementary to the ^{7}Li(p,n)^{7}Be reaction (Ref. 13), the ^{3}H(p,n)^{3}He reaction can also be used for simulating a Maxwell-Boltzmann distribution. Bombardment of a "thick" tritium target (proton energy loss in the target >80 keV) with protons of 1099 keV energy provides a kinematically collimated neutron spectrum within a cone of 120 deg opening angle and with a maximum neutron energy of 225 keV. The integrated distribution corresponds closely to a thermal spectrum of $kT=52$ keV. Compared to the ^{7}Li(p,n) reaction, which yields a spectrum similar to $kT=25$ keV, the neutron intensity from the ^{3}H(p,n) reaction is lower by factors of 10—20.

(ii) The partial capture cross section of ^{84}Kr for populating the isomer in ^{85}Kr and the total capture cross section of ^{86}Kr have been measured in the newly established quasistellar spectrum of $kT=52$ keV as well as in the before known of $kT=25$ keV. The respective stellar cross sections at the standard s-process energy of $kT=30$ keV were determined by interpolation with an overall uncertainty of $\sim7\%$.

(iii) As the new cross sections agree within errors with the data used in a recent analysis of the s-process branching at ^{85}Kr (Ref. 13), the conclusions obtained in that work still hold, with a tendency towards a slightly lower neutron density for the weak s-process component. For a significantly improved analysis of the ^{85}Kr branching, an experimental determination of the ^{85}Kr cross section would be needed.

[1]J. H. Gibbons and R. L. Macklin, Phys. Rev. **159**, 1007 (1967); see also R. L. Macklin, in *Neutron Capture Gamma Ray Spectroscopy*, edited by R. E. Chrien and W. R. Kane (Plenum, New York, 1979), p. 475.

[2]F. Käppeler, K. Wisshak, and L. D. Hong, Nucl. Sci. Eng. **84**, 234 (1983).

[3]H. Beer and F. Käppeler, Phys. Rev. C **21**, 534 (1980).

[4]H. Beer, private communication.

[5]Z. Y. Bao, and F. Käppeler, At. Data Nucl. Data Tables (to be published).

[6]H. Beer and F. Käppeler, in *Neutron Capture Gamma-Ray Spectroscopy and Related Topics*, edited by T. von Egidy, F. Gönnenwein, and B. Maier (Institute of Physics, Bristol, 1982), p. 558.

[7]R.-D. Penzhorn, G. Walter, and H. Beer, Z. Naturforsch. **38a**, 712 (1983).

[8]WM. J. Veigele, At. Data Tables **5**, 51 (1973).

[9]*Table of Isotopes,* edited by C. M. Lederer, V. S. Shirley (Wiley, New York, 1978).

[10]R. L. Macklin, private communication.

[11]R. L. Macklin, J. Halperin, and R. R. Winters, Phys. Rev. C **11**, 1279 (1975).

[12]F. Käppeler, G. Walter, and G. J. Mathews, Astrophys. J. **291**, 319 (1985).

[13]G. Walter, H. Beer, F. Käppeler, and R.-D. Penzhorn, Astron. Astrophys. **155**, 247 (1986).

[14]S. Raman, B. Vogelberg, J. A. Harvey, R. L. Macklin, P. H. Stelson, A. Schröder, and K.-L. Kratz, Phys. Rev. C **28**, 602 (1983).

[15]G. Walter, B. Leugers, F. Käppeler, Z. Y. Bao, G. Reffo, and F. Fabbri, Nucl. Sci. Eng. **93**, 357 (1986).